This is a preprint, the final version is subject to change, of the American Mineralogist (MSA)
Cite as Authors (Year) Title. American Mineralogist, in press.
DOI: https://doi.org/10.2138/am-2020-7168

Revision 2

Radiation-induced defects in montebrasite: an electron paramagnetic resonance study of O^- hole and Ti^{3+} electron centers

José R. Toledo[1], Raphaela de Oliveira[1], Lorena N. Dias[1], Mário L.C. Chaves[2], Joachim Karfunkel[2], Ricardo Scholz[3], Maurício V.B. Pinheiro[1] and Klaus Krambrock[1]*

[1]Universidade Federal de Minas Gerais, Departamento de Física, ICEx, CP 702, 30.123-970 Belo Horizonte, MG, Brazil

[2]Universidade Federal de Minas Gerais, Instituto de Geociências, MG, Brazil

[3]Universidade Federal de Ouro Preto, MG, Brazil

Abstract

Montebrasite is a lithium aluminum phosphate mineral with the chemical formula $LiAlPO_4(F_x,OH_{1-x})$ and considered a rare gemstone material when presenting good crystallinity. In general, montebrasite is colorless, sometimes pale yellow or pale blue. Many minerals that do not have color contain hydroxyl ions in their crystal structure can develop color centers after ionization or particle irradiation, examples of which are topaz, quartz and tourmaline. The color centers in these minerals are often related to O^- hole centers, where the color is produced by bound small polarons inducing absorption bands in the near UV to the visible spectral range. In this work, colorless montebrasite specimens from Minas Gerais state, Brazil, were investigated by electron paramagnetic resonance (EPR) for radiation–induced defects and color centers. Although gamma irradiation (up to a total dose of 1 MGy) did not visibly modify color, a 10 MeV electron irradiation (80 MGy) induced a pale greenish-blue color. Using EPR, O^- hole centers were identified in both gamma- or electron-irradiated montebrasite samples showing superhyperfine interactions with two nearly equivalent ^{27}Al nuclei. In addition, two different Ti^{3+} electron centers were also observed.

From the gamma irradiation dose dependency and thermal stability experiments, it is concluded that production of O^- hole centers is limited by simultaneous creation of Ti^{3+} electron centers located between two equivalent hydroxyl molecules. In contrast, the concentration of O^- hole centers can be strongly increased by high-dose electron irradiation independent of the type of Ti^{3+} electron centers. From detailed analysis of the EPR angular rotation patterns, microscopic models for the O^- hole and Ti^{3+} electron centers are presented, as well as their role in the formation of color centers discussed and compared to other mineral specimen.

Keywords: montebrasite, EPR, irradiation, electron-hole center, O^- hole center, Ti^{3+}, color enhancement.

*Corresponding author: Prof. Klaus Krambrock,: Departamento de Física, Universidade Federal de Minas Gerais, Belo Horizonte, MG, Brazil, e-mail: klaus@fisica.ufmg.br

INTRODUCTION

Nowadays, most gemstone minerals receive color improvements by radiation and/or thermal treatments to transform uncolored to colored material. The color-enhancement procedures leave the gemstones more attractive with increased market values. While radiation treatments induce color centers, in general, heat treatments anneal them out. In some very few cases, heat may also be used to facilitate diffusion processes, which induce color in surface of gemstones (Nassau 2001). Most common radiation treatments for color-enhancement of gemstones make use of ionization radiation, such as gamma irradiation from a ^{60}Co source, or high-energetic electrons from a linear Van-de-Graaff accelerator. Ionization radiation frequently induces electron and hole centers localized near impurity centers. In addition, electron irradiation, as well as other particle irradiation like high-energetic protons or neutrons, may produce also Frenkel pairs, i.e. correlated vacancy and interstitial defects, by atomic displacements in the crystal lattice.

Electron paramagnetic resonance (EPR) is the technique of choice used to identify radiation-induced defects, which are in most cases paramagnetic in nature and often induce color changes in gemstones. For example, some Fe- or Al-containing quartz minerals turn violet (amethyst) or smoky-colored, respectively, by gamma irradiation. A color change in quartz can also be induced by 200°C – 300°C thermal treatments, which may result in brown, orange, yellow or green coloration. In contrast, electron or neutron irradiation is the best choice to produce the deep blue colors (Swiss and London blue) in otherwise colorless topaz, whereas gamma irradiation is chosen only for topaz from very specific locations, and even so the color is much less intense (Sky blue).

One of the most important color centers in gemstone minerals is the O^- hole center, which acts as a bound small polaron (Schirmer 2006). Due to its charge transfer process, small concentrations of such O^- hole centers may induce medium to saturated colors with an absorption band centered in the near UV or the VIS spectral region. For example, the brown and blue colors in topaz (Silva et al. 2005; Krambrock et al. 2007), the irradiation-induced yellow color in tourmaline (Krambrock et al. 2004) and the smoky color in Al-containing quartz are all caused by O^- hole

centers (Meyer et al. 1984). It is important to note that the generation of O^- hole centers by ionization radiation is in general limited by available electron centers, whereas O^- hole centers produced by electron irradiation do not depend on them. The effect of O^- hole centers on inducing different coloration in minerals is still under investigation owing to mixed results. For example, O^- hole centers are known to form in Brazilianite, and because of the firm localization of the hole (Requardt et al. 1982) it appears to introduce only absorption bands outside the visible spectrum in the near UV with a band tail entering the visible spectral range that still results in a yellow color. For euclase, the O^- centers are present but the mineral is still colorless. As mentioned before, many minerals that contain hydroxyl ions in their crystal structure are known to form O^- hole centers following irradiation, such as topaz $Al_2SiO_4(F,OH)_2$ (Silva et al. 2005; Krambrock et al. 2007), apatite $Ca_5(PO_4)_3(OH,F,Cl)$ (Mengeot et al. 1975), jeremejevite $Al_6B_5O_{15}(F,OH)_3$ (Li et al. 2012), tourmaline-elbaite $Na(Li,Al)_3Al_6(BO_3)_3$ $Si_6O_{18}(OH)_4$ (Krambrock et al. 2004) and kaolinite $Al(SiO_5(OH)_4)$ (Clozel et al. 1995) . This is also the case for the montebrasite (Bershov and Martirosyan 1970) which is investigated in this work.

Montebrasite has a triclinic structure (C_1). The structure is characterized by corner sharing distorted Al octahedra, which are interconnected along the ***c***-axis by (F, OH) ions. Laterally, these are cross-linked by nearly perfect PO_4 tetrahedra. The octahedra and tetrahedra form cavities, which are occupied by Li ions in two slightly different off-center positions. Also, the two Al octahedra within the primitive unit cell, $Al(1)O_4(F,OH)_2$ and $Al(2)O_4(F,OH)_2$, are structurally slightly different. For the first octahedra, the distances to the oxygen ligands are 1.900, 1.899 and 1.918 Å, while for the second they are 1.906, 1.856 and 1.920 Å (Groat et al. 2003). If the Li off-center positions are omitted the space group of montebrasite may be described as monoclinic, similar to that of titanite with cell parameters: ***a*** = 6.713 (6.645), ***b*** = 7.708 (7.733) and ***c*** = 7.019 (6.919) Å with β = 117.93° (117.44°) (Groat et al. 1990).

In this work, both gamma and electron irradiation are used to study the formation of O^- hole centers and to see whether these centers may cause color changes in montebrasite. Previous single-

crystal electron paramagnetic resonance (EPR) investigations of natural montebrasite samples from Brazil revealed the presence of different transition metal-related impurities such as iron, vanadium and niobium all substituting for octahedral Al^{3+} ions (Dias et al. 2011). Most of these samples were colorless at neutral conditions, prior to any irradiation or heat treatments, indicating that the transition metal ions have, due to their low concentrations, only a negligible influence on the color. In many cases, color transitions can also be induced by rare earths following high energy irradiation, but this is not the case since rare earth ions, at sufficient concentrations for that, have not been observed before in montebrasite. In this study, detailed EPR investigations of gamma and electron irradiation-induced effects and defects are presented. A dominant O^- hole center, often found after irradiation in many minerals, is analyzed together with two different Ti^{3+} electron centers. Based on the EPR spin Hamiltonian parameters found for these centers, and on their estimated concentration, as well as their behavior with radiation dose and heat, a model for the formation process of the irradiation-induced defects is proposed, and the color enhancement processes are discussed.

EXPERIMENTAL

All the samples studied in this work have been analyzed before for impurities (Dias et al. 2011). Previous investigations have shown that the montebrasite samples used in this study are OH-rich with low content of fluorine anions (OH^- 96%; F^- 4%). Naturally colorless and pale yellow-colored single crystal specimens of montebrasite from the Linópolis area in the Divino das Laranjeiras municipality of Minas Gerais state (Brazil) were chosen for our investigation. Samples were oriented using the perfect cleavage plane (100), cut and polished to parallelepipeds of about 3 x 3 x 3 mm^3. Gamma irradiations were performed using a panoramic ^{60}Co source (CDTN, Belo Horizonte, Brazil) with flux of 15 kGy/h and total dose ranging from 10 to 1000 kGy. Electron irradiations under water cooling were performed with a linear Van de Graaff accelerator (Aceletron,

Rio de Janeiro, Brazil) with a total dose of 80 MGy. Isochronal annealing experiments were done in a conventional tubular furnace (Lindberg Blue) at ambient atmospheres.

EPR experiments were carried out on a modified Miniscope 400 spectrometer using the X-band (9.44 GHz) for analysis (Magnettech, Germany). The automated microwave bridge is coupled to a rectangular microwave resonator that is inserted into a 9'' electromagnet (Varian, USA). A low voltage, high current source (Walker, USA) allows magnetic field scans from 0 to 0.8 T. The resonator is mounted on a Helium flux cryosystem ESR-900 (Oxford, England) that permits sample temperatures ranging between 4.2 to 300 K. The samples are fixed to a sample holder, which coupled to an automated goniometer allowed for measuring angular dependencies in one plane with high precision. Typical EPR measurements of the irradiation-induced defects in single-crystalline montebrasite samples were performed in the temperature range from 10 to 300 K, using a 330 mT center field, sweep range of about 60 mT, 100 kHz modulation, field modulation of about 0.2 mT, resulting in a scan time of about 1 min. For some of the experiments, after each irradiation step, the samples were measured and, in the sequence, thermally treated at about 400°C, before a new irradiation dose was applied. In most cases, due to the high sensitivity of our EPR spectrometer, one EPR scan was enough for a very good signal-to-noise ratio. The DPPH (1,1-Diphenyl-2-Picrylhydrazyl) marker was used for calibration of the *g* factors ($g = 2.0037$).

EXPERIMENTAL RESULTS

The present work study electron and hole centers produced by radiation and their thermal stability apart from the radiation-induced color changes in montebrasite. For this study we have choosen specifically those colorless samples denoted AAM in our previous publication (Dias et al. 2011), that presented only EPR spectra due to Fe^{3+} and VO^{2+} impurities in low concentration for non-irradiated montebrasite crystals.

Figures 1 (a, b, c) present the room-temperature EPR spectra of sample AAM measured in the natural state, after gamma irradiation with a dose of 200 kGy and electron irradiation with a

dose of 80 MGy, respectively. The EPR spectra were measured with the magnetic field aligned with the a-axis of montebrasite. After gamma irradiation, two paramagnetic defects dominate the EPR at room temperature (Figure 1b). Based on the spin Hamiltonian parameters, as it will be shown later, one is due to an O^- hole center and the other due to Ti^{3+} electron center. These two paramagnetic centers were also detected with low intensity in the natural samples together with the VO^{2+} center (Figure 1a). Finally, the EPR spectrum of the electron-irradiated sample is dominated by the O^- hole center (Figure 1c).

The EPR spectrum of the O^- hole centers shows eleven lines with intensity ratios, confirmed later by a lineshape analysis, of approximately 1:2:3:4:5:6:5:4:3:2:1. Such EPR spectrum is expected for a spin $S = 1/2$ paramagnetic center showing superhyperfine (shf) interaction with two equivalent nuclear spins $I = 5/2$. The montebrasite with two formula units per unit cell ($Z = 2$) and chemical formula $LiAl(PO_4)(F_{0.04},OH_{0.96})$ has two nearly equivalent ^{27}Al nuclei ($I = 5/2$, 100% abundance). Figure 1d presents the measured EPR spectrum compared with that of a fit using the Easyspin@ software (Stoll and Schweiger 2006) for an O^- center interacting with two equivalent ^{27}Al nuclei.

The EPR spectrum of the Ti^{3+}(I) electron center, measured at room temperature in the gamma irradiated sample, consists of three dominant EPR lines with intensity ratio of 1:2:1 (Figure 1e). The identification of this center with Ti^{3+} ions ($3d^1$: $S = 1/2$) is based on the hyperfine interaction due to the two Ti isotopes with nuclear spins ^{47}Ti ($I = 5/2$, 7.4 % abundance) and ^{49}Ti ($I = 7/2$, 5.4 % abundance). These two isotopes produce six and eight low-intense satellite lines (Figure 1e). This room temperature Ti-related electron center was labeled Ti^{3+}(I). Considering charge and ionic radii, the Ti^{3+} ions are expected to replace Al^{3+} ions in the montebrasite structure, which are diamagnetic (Ti^{4+}) prior to irradiation. The intensity ratio of 1:2:1 of the EPR lines is characteristic for superhyperfine (shf) interaction with two equivalent nuclei with nuclear spin $I = 1/2$, which in montebrasite may be due to the interaction of two equivalent ^{19}F or two ^1H nuclei from hydroxyl OH^- ions. Furthermore, double integration of the EPR spectra of O^- and of Ti^{3+} ions

in the gamma-irradiated sample shows that the concentration of both the O^- hole centers and the Ti^{3+}(I) electron centers are nearly the same. This observation can be explained if an O^{2-} impurity ion replaces a regular OH^- or F^- ion, and gamma irradiation is capable of transferring an electron from it to the Ti^{4+} ion forming O^- hole centers and Ti^{3+} electron centers.

The EPR spectrum in Figure 1c for the electron-irradiated sample is dominated by the O^- hole centers showing again 11 lines due to interaction of two nearly equivalent ^{27}Al nuclei. The lineshape of this spectrum is identical to the one of the O^- centers produced by gamma-irradiation. The absolute intensity after double integration of the derivative-like EPR spectrum shows that the concentration of the O^- centers is, for comparison purposes, about a factor of five times higher compared to that obtained with gamma irradiation. It is also important to note that electron irradiation did not induce a significant concentration paramagnetic Ti^{3+}(I) electron centers.

Low-temperature EPR measurements (15 K) showed that all samples (non-irradiated, gamma-, and e-irradiated) contain other Ti^{3+} electron center (see for example, Figure 1f) as identified also by the hyperfine satellite lines of the two Ti isotopes ^{47}Ti and ^{49}Ti. This Ti^{3+} electron center has a different *g* factor and does not show the shf interaction with two equivalent nuclei with $I = 1/2$. It was labeled Ti^{3+}(II) and its intensity was not changed by the irradiation procedure.

For the analysis of the EPR spectra of the different paramagnetic centers shown in Figures 1(d-f), the EPR spectra were first analyzed individually. For that, the Easyspin@ software was used by taking into account the following spin Hamiltonian in triclinic symmetry:

$$H = \beta \boldsymbol{S} g \boldsymbol{B} + \sum_i (\boldsymbol{S} A \boldsymbol{I}_i - \beta_n \boldsymbol{I}_i g_n \boldsymbol{B}) \quad (1)$$

In eq. 1, the first term represents the electronic Zeeman interaction, the second the hyperfine (hf) and/or superhyperfine (shf) interaction and the third the nuclear Zeeman interaction. Quadrupole interaction was omitted. The symbols have their usual meaning in the EPR literature (Spaeth et al. 1992). For the individual EPR spectra, fits with Voigt line shapes (mix of Lorentzian/Gaussian) were used.

In order to analyze the geometry, symmetry and magnetic interactions of the different radiation-induced paramagnetic centers in montebrasite, EPR angular dependencies were measured in three mutually perpendicular crystal planes defined as the P1: ***c*b*c****, P2: ***c*ac**** and P3: ***b*ab**** planes. The asterisks conventionally indicate directions that are perpendicular to others. The EPR angular dependencies are shown in Figures 2(a-c) for the O^- and the Ti^{3+}(I) present in gamma-irradiated sample, and in Figures 2(d-f) for the Ti^{3+}(II) spectra measured at low temperature (15 K) in electron-irradiated sample. Within the measurement accuracy, and taking into account small frequency shifts for the incident microwave, the O^- center produced by electron irradiation has the same EPR angular dependence compared with that after gamma irradiation.

The shf interactions of the two Al nuclei are not always fully resolved (Figures 2(a-c)). In order to get the symmetry of the *g* tensor representative of the O^- hole centers, the central positions of the individual EPR lines (denoted as line positions) were determined directly from the spectra as a function of sample orientation. Then, the line positions were fitted simultaneously, using a least squares fit procedure, for the three mutual perpendicular planes, with the appropriate spin Hamiltonian within the EPRNMR$^{@}$ software (Mombourquette and Weil 2006). The results of such an analysis are presented in Figure 3 where the dots correspond to measured line positions, and the red solid lines the fits for the O^-, Ti^{3+}(I) and Ti^{3+}(II) centers. The spin Hamiltonian parameters were determined by the simultaneous fit of all line positions in the three perpendicular crystal planes using exact diagonalization of the spin Hamiltonian. Table 1 lists the spin Hamiltonian parameters and their errors that resulted from this analysis. For the O^- center, the angular dependencies were identical for both the gamma-irradiated and electron-irradiated samples.

The symmetry of the *g* tensor of the O^- hole center is not pseudo-axial as frequently observed, but is clearly indicative of low symmetry (orthorhombic or less). The principal directions of the *g* tensor are indicated in Figure 3(a-c). Table 1 lists the spin Hamiltonian parameters and its principal directions in polar coordinates measured from the *a*-axis. It is important to note that g_{zz} is nearly aligned with the diagonal of the *ab* plane and most importantly, nearly perpendicular to the

220 ***c***-axis, as expected considering that the hole resides in a p-orbital. Although the line position plots
221 shown in Figure 3 present only one of the two inequivalent sites (Z = 2 for montebrasite) in each of
222 the three mutually perpendicular planes, individual spectral fits indicated that, for some
223 orientations, at least two inequivalent sites with very similar spin Hamiltonian parameters had to be
224 included in the analysis. However, due to the low resolution in the spectra only one site was
225 analyzed.

226 The superhyperfine (shf) interaction with the two nearly equivalent ^{27}Al nuclei of the O^-
227 hole centers was also not well-resolved for all crystal orientations. The shf interaction is much
228 smaller than the electronic Zeeman interaction. Therefore, first order perturbation theory may be
229 applied. Analyzing the individual EPR spectra in the three crystal planes and assuming pseudo-axial
230 symmetry of the shf interaction tensor, the maximum and minimum values of the shf interaction can
231 be estimated, where shf_{max} and shf_{min} correspond to $(a + 2b) = 0.805(3)$ mT and $(a - b) = 0.687(2)$
232 mT values, respectively. From these values, the isotropic and uniaxial components of the shf tensor
233 *a* and *b* are obtained. Their principal values (in MHz) are also listed in the Table 1. The analysis
234 shows that the principal direction of the shf interaction is nearly along the ***c***-axis, i.e. more exactly
235 (***c*** + 20º) in the *ac* plane. The analysis also shows that the anisotropic shf interaction *b* (dipole
236 interaction) is only about 6% of the isotropic interaction *a*. Such values are frequently observed for
237 O^- hole centers in minerals and will be discussed below.

238 The EPR spectra of the angular dependencies of the two Ti^{3+} electron centers Ti^{3+}(I) at 300
239 K and Ti^{3+}(II) at 15 K were also analyzed in detail, using a similar approach as that used for the O^-
240 center. They are shown in the Figures 3(d-f) and 3(g-i), respectively. As mentioned before, the
241 identification of these centers was based on a lineshape analysis with a spin Hamiltonian that
242 includes a hyperfine interaction of the unpaired electron with the two titanium isotopes ^{47}Ti (I = 5/2,
243 7.4 %) and ^{49}Ti (I = 7/2, 5.4 %). This model perfectly adjusted the EPR lineshapes producing 6 and
244 8 hf satellite lines, respectively, with expected intensity ratios due to the natural, isotopic
245 abundances. Figure 1e shows the measured EPR spectrum of the Ti^{3+}(I) center with three shf lines

for $\boldsymbol{B} \parallel \boldsymbol{a}$ together with a fit of the spectrum including the hyperfine interaction due to the Ti isotopes. The *g* factor for this direction is 1.9400, typical for an electron center with negative *g* shift in relation to g_e (Pake and Estle 1973). The hyperfine interaction of the Ti isotopes is $a(^{47}\text{Ti})/h$ = 46.5(1) MHz (the nuclear *g* factors are nearly the same for both Ti isotopes ^{47}Ti and ^{49}Ti) and the shf interaction of two equivalent protons (^{1}H) is $a(^1\text{H})/h$ = 24.9(1) MHz. It is important to mention that the signs of the hyperfine/superhyperfine coupling constants are associated with the distribution of the electron/hole wavefunctions over the nuclear spins involved in the interactions. In the case of the ^{1}H and ^{47,49}Ti hyperfine interactions, and unlike for the O^- interaction with two nearly equivalent ^{27}Al nuclei, the isotropic hf parameter is positive, consistent with the fact that the orbital occupied by the unpaired electron of the Ti atom points directly towards the hydrogen nuclei.

The dominant fingerprint of the Ti^{3+}(I) EPR spectra is the intensity ratio of 1:2:1 of three EPR lines indicating the shf interaction with two equivalent nuclei with nuclear spin $I = 1/2$. Figures 3 (d-f) show the angular dependencies of the experimental EPR line positions (black circles) together with the calculated fits (red solid lines) of the spin Hamiltonian from eq. 1. The fit shows good agreement with the measured line positions. The *g* tensor of this Ti^{3+}(I) center shows low symmetry, indicating an orthorhombic or even lower symmetry. The central line of the EPR spectra always shows twice the intensity of the two satellite lines. The spectra are consistent with Ti^{3+} substituting for Al^{3+} ions in the montebrasite structure. The spin Hamiltonian parameters of the Ti^{3+}(I) center used in the fit (red lines in Figures 3(d-f)) are also shown in Table 1. The principal value g_{zz} is nearly aligned with the diagonal of the *ab* plane, while the principal value of the shf tensor ($A_{zz} = A_{\parallel} = a + 2b)/h$ is pointing approximately along the direction of the bond between Ti_{Al} and the two protons from next nearest neighbor hydroxyl ions. If two equivalent fluorine neighbors would originate the shf interaction, the maximum shf interaction should be expected, due to the atomic arrangement in the montebrasite crystal structure, to be aligned nearly with the ***c***-axis, which is not the case. Therefore, we conclude that the Ti^{3+}(I) center is substituting Al^{3+} ions with two equivalent OH^- neighbors.

The second Ti^{3+} center, labeled Ti^{3+}(II), has spin Hamiltonian parameters of g = 1.8090(1) and $a(^{47}Ti)/h$ = 83.1(1) MHz when the magnetic field is along the ***a***-axis (see Figure 1f). This center does not show any resolved shf interaction with two equivalent protons, at least within the individual linewidth. Sections of the measured EPR angular dependencies of this center are shown in Figure 2(c-e) for the three mutually perpendicular crystal planes of the electron-irradiated sample, measured at the low temperature of 15 K. At this temperature, the EPR spectra of the O^- hole center are slightly saturated since their individual lines are broadened and the overall lineshape is changed. Figures 3(g-i) represent the line positions of the EPR angular dependencies, together with a fit of the g tensor. The spin Hamiltonian parameters of Ti^{3+}(II) are also listed in Table 1.

The analysis shows that the anisotropy of the g tensor of Ti^{3+}(II) is much more strongly distorted, and that the principal direction of the g tensor is nearly aligned with the a-axis. From charge and ionic radius considerations, this Ti^{3+} center should also replace Al^{3+} ions in the montebrasite structure. The missing shf interaction with two equivalent ^{19}F or ^{1}H might be explained if we assume that this Ti^{3+} center substitutes for Al^{3+} where the nearest neighbors are O^{2-} ions substituting for OH^- or F^- ions along the ***c***-axis. These two extra negative charges might compensate two extra positive charges of impurity ions like, for example, the V^{5+} substituting for Al^{3+}, remembering that vanadium as impurity has also been detected with EPR, as V^{4+} hole center (Dias et al. 2011).

Correlation experiments including irradiation dose dependence and isochronal annealing show that impurity ions and intrinsic defects may exchange charges. Figure 4a and 4b show the concentrations in ppm (wt.) of the O^- and Ti^{3+}(I) centers in the AAM sample as a function of gamma irradiation dose and of the isochronal (30 min.) annealing temperature, respectively.

Figure 4a shows that concentrations of the O^- and Ti^{3+}(I) are influenced by gamma irradiation dose. As mentioned before, the concentration of both centers was calculated by double integration of the EPR spectra with its usual uncertainties reproduced in the error bars (Schmitz et al. 1979). It is clear that the concentration of both O^- and Ti^{3+}(I) increases with the gamma

irradiation dose between 0 and 100 kGy, after it saturates. Isochronal annealing experiments in the 200 – 300ºC temperature range simply invert this behavior; the concentrations of both centers are thermally stable until approximately 150°C after which they were drastically reduced. At 300°C, both irradiation-induced centers disappeared. Figure 4 shows also that both O^- and Ti^{3+} centers are of the same order of concentration (~ 10 ppm wt.%). For quantification and calibration of the EPR spectra a $CuSO_4 \cdot 5H_2O$ concentration standard was used.

Figure 5 shows the optical absorption spectra of the non-irradiated and the e^--irradiated montebrasite sample. The spectrum of the gamma-irradiated sample, which is omitted for clarity, is similar to that of the natural non-irradiated sample with negligible absorbance in the visible range and only a slightly higher absorption in UV spectral region. The absorption spectrum of the high-dose (80 MGy) electron-irradiated sample is strongly increased in the UV spectral region, doubling the absorbance from 0.6 up to 1.35 at 350 nm. This change in the UV absorbance is also reflected in the blue spectral region of the visible spectrum and is accompanied by the appearance of a low-intense absorption band in the yellow spectral region (580 nm). Both absorption bands form an absorbance valley between 425 and 525 nm leaving the sample with a pale greenish-blue color (see insert in the Figure 5). Gamma irradiation did not modify the color for the doses applied (up to 1 MGy), and the sample was still without color after irradiation. In contrast, electron irradiation (10 MeV) up to a dose of 80 MGy turned the sample pale greenish-blue.

DISCUSSIONS

Two types of O^- hole-centers are distinguishable according to the classification scheme by Marfunin (Marfunin 1979). There are O^- centers that can be formed by irradiation from oxygen impurities such as oxygen substituting for halogen ions like F^- in apatite $Ca_5(PO_4)_3(F,OH,Cl)$, or in silicate minerals where the O^- is nearby an impurity/defect. One well-known example for the latter is the Si-O^--Al center in smoky quartz. In general, the *g* factors of the O^- centers are often axial or pseudo-axial. This first type of O^- center according to Marfunin (Marfunin 1979) belongs to the σ

variety with $g_{\parallel} < g_e$ and $g_{\perp} > g_e$, while the other belongs to the π variety with inverted g-factor shifts (Marfunin 1979). For both, often a superhyperfine structure due to neighbor nuclei is observed. One type of O^- hole center, for example, which is confirmed to be responsible for the dark blue color (commonly known as London-blue) in neutron-irradiated topaz, is formed on normal OH^- lattice sites (Silva et al. 2005). However, the classification scheme of Marfunin does not describe perfectly this color center in topaz, because the deviation of the g-factor from that of free electron is unusually large. Even though, the g values of the O^- hole center in montebrasite are closely comparable to those in jeremejevite (Li et al. 2012) and kaolinite (Clozel et al. 1995)). These O^- centers, together with that in neutron-irradiated topaz can still be considered as variants of Marfunin's second type, i.e. those known as π-type. The strong deviation from the axial symmetry of these O- hole centers has been attributed by Schirmer (Schirmer 2006) to a spontaneous distortion followed by a symmetry reduction in the ground state compatible with a static Jahn-Teller effect (Li et al. 2012).

Other similarity of the O^- center in montebrasite with the O^- color centers in the neutron-irradiated blue topaz (Silva et al. 2005) has to do with charge compensation. In both cases, the charge compensating electron centers are probably being created in very high concentrations by these high-energetic particle irradiations, independent on the sample´s origin and on the impurity content (Krambrock et al. 2007). To some extent, the electron centers do indeed exist in low concentrations in natural topaz, because of natural irradiation over long geological times. However, when we consider the EPR results for the O^- center in montebrasite produced by electron irradiation, and also for the London-blue topaz (Silva et al. 2005), there must be some kind of charge compensating electron center, though not paramagnetic, at sufficient concentrations to guarantee charge neutrality of the lattice.

In most minerals with structural OH^- groups in the lattice, as those listed above in the introduction, the O^- center formation by particle irradiation involves kicking off hydrogen atoms H^0 by inelastic collisions, leaving behind O^- hole centers (Hill and Lehmann 1978; Krambrock et al.

2004; Silva et al. 2005). Depending on the radiation energy or temperature, atomic hydrogen centers are frequently unstable at room temperature and form neutral molecular H_2 (Krambrock et al. 2004).

In several minerals, regardless of whether they are oxides, ionization radiation may produce O^- hole centers. More precisely, they are produced by gamma irradiation in a completely different way, as for example is the case for euclase (Dias et al. 2009). The O^- hole centers in euclase are formed by a metastable charge transfer transition, in which nearby point defects capture the extra electron forming an electron centers, i.e. Ti^{3+}. Commonly, these point defects are substitutional transition metal impurities, which may exist in different charge states or, on the other hand, intrinsic defects like vacancies. However atomic hydrogen H^0, which may be produced directly by particle irradiation from the breakdown of OH^- groups, is representing an electron trap (Hill and Lehmann 1978; Krambrock et al. 2004). In the case of ionizing radiation, the charge transfer is metastable and can be reversed by heat, usually for thermal treatments above room temperature, and recreated after irradiation. Despite the processes are different, the result is usually the same O^- center, independent of the type of radiation. There is, however, a strong difference in the two processes with respect to the overall concentration of the O^- centers. For the charge transfer process, the concentration of the O^- hole centers is limited by the available amount of electron traps due to impurities. For particle irradiation, the O^- are produced in the lattice together with the electron traps. This is why the colors produced by gamma irradiation are usually paler than those produced by high-energetic electrons, and why the colors get saturated at doses around 100 to 200 kGy by the concomitant formation of charge compensating electron centers.

In this work, the investigation of radiation-induced defects in gamma-irradiated samples by EPR allowed for the identification of an O^- hole center with two nearly equivalent Al neighbors, as shown in the Figure 6. Figure 6a shows the atomic arrangement of the O^- hole center together with the principal directions of the its *g* and Al shf tensor. As expected, the *p*-orbital of the O^- hole center represented by the principal direction of the *g* tensor is nearly perpendicular to the connection line

of the two equivalent Al neighbors, meaning that it is nearly aligned with the diagonal of the *ab* plane, and perpendicular to the ***c***-axis. On the other hand, the principal direction of the shf tensor is oriented along the (***c*** + 20º) in the *ac* plane. The small anisotropic shf interaction *b*, about 6%, and the large isotropic shf interaction *a* of the O^- center, which should be negative, is explained consistently by the theory of exchange polarization transferred hyperfine interaction (Adrian et al. 1985). Both the isotropic and anisotropic ^{27}Al shf values for the O^- center in montebrasite, (*a* = -18.1 MHz and *b* = 1.1 MHz), are similar, albeit slightly smaller, to the ones obtained for O^- centers in yellow tourmaline (*a* = -23.2 MHz and *b* = 0.6 MHz) (Krambrock et al. 2004), blue topaz (*a* = -26.6 MHz and *b* = 1.3 MHz) (Silva et al. 2005) and jeremejevite (Li et al. 2012). For the latter, by means of a combination of experimental EPR results and theoretical DFT calculations, the shf tensor components were found to A_1 = -0.881 mT, A_2 = -0.951 mT and A_3 = -0.972 mT with an isotropic shf parameter a of about *a* = -26 MHz) (Li et al. 2012).

Figures 6b and 6c show respectively the atomic arrangements of the two Ti-related electron centers Ti^{3+}(I) and Ti^{3+}(II). Both were identified by their central hf interaction due to the isotopes ^{47}Ti (*I* = 5/2, 7.4 %) and ^{49}Ti (*I* = 7/2, 5.4 %) and assumed to substitute for Al^{3+} ions. Both Ti^{3+} -related centers, Ti^{3+}(I) and Ti^{3+}(II), show low symmetry, compatible with the triclinic structure of montebrasite. Both centers have *g* values with a negative *g* shift in relation with that of the free electron, indicating that they indeed represent electron centers (Pake and Estle 1973). Although it is difficult to interpret the principal directions of the *g* tensors of both Ti^{3+}-related electron centers, the EPR spectra of the Ti^{3+}(I) center present a splitting due to the interaction of two equivalent nuclei with nuclear spins of *I* = ½. These two equivalent nuclei are identified as two equivalent protons from hydroxyl ions next to Ti due to the orientation of the principal axis of the shf tensor, which is pointing nearly along the diagonal in the *ab* plane. If the two equivalent nuclei would be fluorine, the principal axis should point nearly along the ***c***-axis, which is not the case. The principal axes of the interaction tensors of both Ti-related centers, Ti^{3+}(I) and Ti^{3+}(II), are shown in the Figures 6b and 6c, respectively.

Because the Ti^{3+}(II) center does not present the shf interaction with two equivalent nuclear spins I = 1/2, we assume that Ti^{3+}(II) has two impurity O^{2-} neighbors, instead of two OH^- or F^- neighbors. Different to the Ti^{3+}(I) center, the g tensor of Ti^{3+}(II) is much more distorted and the principal axis of its g tensor is nearly aligned with the a-axis (see Figure 6c), which may be caused by an unknown nearby impurity or defect like, for example, Ti pairs in dislocations.

The concentration of the three paramagnetic electron and hole centers were investigated as a function of gamma-irradiation dose and after isochronal annealing (see Figure 4). For the gamma-irradiation, the O^- hole-center concentration seems to be directly related to the concentration of the electron center identified as the room-temperature Ti^{3+}(I) substituting for Al^{3+}, with two nearby hydroxyls, in a very similar way as was observed for euclase (Dias et al. 2011). For gamma irradiation, the concentrations of these two centers saturate in our montebrasite sample at an estimated concentration of about 10 ppm wt., for doses above 100 kGy. On the other hand, for isochronal annealing of the same sample above 200°C, they start to decrease with both centers vanishing totally above 300°C. Since no color is produced after irradiation, we presume that the O^- concentration is below the threshold for inducing measurable absorption bands in the visible range.

The formation of the O^- hole centers along with the Ti^{3+} electron centers by gamma irradiation can be thus summarized as follow:

$$\begin{bmatrix} Al-O^{2-}{}_{OH^-}-Al \\ + \\ OH-Ti^{4+}_{Al}-OH \end{bmatrix}^0 \xrightarrow{\gamma} \begin{bmatrix} Al-O^{-}{}_{OH^-}-Al \\ + \\ OH-Ti^{3+}_{Al}-OH \end{bmatrix}^0 \xrightarrow{300^oC} \begin{bmatrix} Al-O^{2-}{}_{OH^-}-Al \\ + \\ OH-Ti^{4+}_{Al}-OH \end{bmatrix}^0$$

Charge compensation thus, guarantees the overall lattice neutrality. On the other hand, the Ti^{3+}(II) center is observed only at low temperatures in all types of samples: non-irradiated, gamma- and electron-irradiated samples. Its concentration does not dependent on the irradiation type or dose, nor on the annealing temperature. Therefore, it cannot be accounted as a compensating electron center for the O^- hole centers.

A different situation arises in the same sample after high-energetic electron irradiation. The same O^- hole center is created, but without the correlated Ti^{3+}(I) electron center. Besides that, the O^- center concentration is approximately five times higher than that for gamma irradiation, with one absorption band in the near UV and another weaker band at 580 nm appearing simultaneously to the O^- center. These two absorption bands leave a transmittance valley between 450 - 500 nm and originate a pale greenish-blue color (Figure 5). This time an O^- concentration threshold for the color seems to be reached at about 50 ppm wt.% for the electron-irradiated sample. One must bear in mind, however, that this color is not strong since the visible spectrum changes only slightly with the weak intense 580 nm band. The scheme below shows the formation process of O^- centers by electron irradiation:

$$\mathbf{2(Al - OH^-_{OH^-} - Al)} \xrightarrow{e^- \ (80MGy)} \mathbf{2(Al - O^-_{OH^-} - Al)} + \mathbf{2H^0 \rightarrow H_2}$$

It is analogous to that for O^- centers produced by high-energetic electrons and neutrons in topaz (Silva et al. 2005). In this case, the OH^- ions are the source for both, the O^- hole centers and atomic hydrogen, H^0, as the corresponding electron centers. Because H^0 was not detected by EPR, we have to assume that they diffuse and form EPR-silent H_2 molecules. However, in order to investigate the irradiation-induced formation of atomic hydrogen in montebrasite, low-temperature irradiation followed by low-temperature EPR experiments, without heating the samples up to room temperature, would be necessary.

IMPLICATIONS

The implications of the present study are important for color improvements by irradiation and heat in gemstone materials using ionization and electron irradiations. This is particularly relevant for most gemstone minerals that contain hydroxyl ions in their crystalline structure. These implications are important for the identification of the radiation-induced color centers, the factors that stabilize them and the understanding of their optical properties. For many oxide materials, the

irradiation-induced color centers are related with O^- hole centers which are stabilized near acceptor defects. Their identification is done by electron paramagnetic resonance (EPR). The color produced from such O^- hole centers is based on a phenomenological theory and explained by bound small polarons; the trapped hole jumps between equivalent positions in the neighborhood of an acceptor, similar to a charge transfer process inducing optical absorption bands from the near UV to the visible spectral range. In most cases, the stabilizing acceptor for the bound hole is not known. In this context, the microscopic structure and symmetry of three unknown irradiation-induced paramagnetic centers in the rare gemstone montebrasite were identified by EPR from the analysis of their spin Hamiltonian parameters. Two of them, the O^- hole center interacting with two nearest equivalent nuclei from Al^{3+} ions and the Ti^{3+}(I) electron center interacting with two nearby equivalent protons from structural hydroxyl ions are simultaneously created by gamma irradiation and destroyed by heat at about 200 ºC. Both act as a matched pair of charge compensating centers. The maximum gamma irradiation-induced concentration of O^- centers is limited by available electron centers. For this limited O^- hole center concentration, no visible color in the montebrasite was produced. On the other hand, using high-energetic electron irradiation, the O^- hole center concentration was about 5 times higher compared with gamma irradiation. Since no Ti^{3+}(I) electron centers are identified in reasonable concentration in this process, the formation of the O^- centers follows other mechanism, probably related with the formation of atomic hydrogen, H^0, with likely recombination and formation of diamagnetic molecular hydrogen H_2. The O^- centers created by electron irradiation are probably related with a low-intense absorption band centered in the visible spectral range at 580 nm and an intense broad absorption band covering a large UV spectral range, responsible for the pale greenish–blue color. For the correlation of the color with the O^- centers in electron-irradiated samples, as well as the model for charge compensation, and its concentration dependence with irradiation dose and thermal treatments more experiments are required.

ACKNOWLEGDEMENTS

The authors are grateful for financial support from the Brazilian agencies FAPEMIG, CNPq, CAPES and FINEP.

REFERENCES CITED

Adrian, F.J., Jette, A.N., and Spaeth, J.M. (1985) Theory of indirect hyperfine interactions of oxygen-aluminum defects in ionic crystals. Physical Review B, 31, 3923–3931.

Bershov, L. V., and Martirosyan, V.O. (1970) Electron and hole defects in nonirradiated single crystals of natural lithium and aluminum phosphates (ambligonite). Journal of Structural Chemistry, 10, 628–629.

Clozel, B., Gaite, J.-M., and Muller, J.-P. (1995) Al-O--Al paramagnetic defects in kaolinite. Physics and Chemistry of Minerals, 22, 351–356.

Dias, L.N., Pinheiro, M.V.B., and Krambrock, K. (2009) Radiation-induced defects in euclase: formation of O− hole and Ti3+ electron centers. Physics and Chemistry of Minerals, 36, 519–525.

Dias, L.N., Pinheiro, M.V.B., Moreira, R.L., Krambrock, K., Guedes, K.J., Filho, L.A.D.M., Karfunkel, J., Schnellrath, J., and Scholz, R. (2011) Spectroscopic characterization of transition metal impurities in natural montebrasite/amblygonite. American Mineralogist, 96, 42–52.

Groat, L.A., Raudsepp, M., Hawthorne, F.C., Ercit, T.S., Sherriff, B.L., and Hartman, J.S. (1990) The amblygonite-montebrasite series: characterization by single- crystal structure refinement, infrared spectroscopy, and multinuclear MAS-NMR spectroscopy. American Mineralogist, 75, 992–1008.

Groat, L.A., Chakoumakos, B.C., Brouwer, D.H., Hoffman, C.M., Fyfe, C.A., Morell, H., and Schultz, A.J. (2003) The amblygonite (LiAlPO 4 F)-montebrasite (LiAlPO 4 OH) solid solution: A combined powder and single-crystal neutron diffraction and solid-state 6 Li MAS,

499 CP MAS, and REDOR NMR study. American Mineralogist, 88, 195–210.
500 Hill, F., and Lehmann, G. (1978) Atomic Hydrogen in the Mineral Brasilianite
501 NaAl3(PO4)2(OH)4. Zeitschrift fur Naturforschung - Section A Journal of Physical Sciences,
502 33, 1484–1486.
503 Krambrock, K., Pinheiro, M.V.B., Guedes, K.J., Medeiros, S.M., Schweizer, S., and Spaeth, J.-M.
504 (2004) Correlation of irradiation-induced yellow color with the O - hole center in tourmaline.
505 Physics and Chemistry of Minerals, 31, 168–175.
506 Krambrock, K., Ribeiro, L.G.M., Pinheiro, M.V.B., Leal, A.S., Menezes, M.Â. de B.C., and Spaeth,
507 J.-M. (2007) Color centers in topaz: comparison between neutron and gamma irradiation.
508 Physics and Chemistry of Minerals, 34, 437–444.
509 Li, R., Li, Z., and Pan, Y. (2012) Single-crystal EPR and DFT study of a VIAl–O−–VIAl center in
510 jeremejevite: electronic structure and 27Al hyperfine constants. Physics and Chemistry of
511 Minerals, 39, 491–501.
512 Marfunin, A.S. (1979) Spectroscopy, Luminescence and Radiation Centers in Minerals. Springer
513 Berlin Heidelberg.
514 Mengeot, M., Bartram, R.H., and Gilliam, O.R. (1975) Paramagnetic holelike defect in irradiated
515 calcium hydroxyapatite single crystals. Physical Review B, 11, 4110–4124.
516 Meyer, B.K., Lohse, F., Spaeth, J.M., and Weil, J.A. (1984) Optically detected magnetic resonance
517 of the (AlO4)0 centre in crystalline quartz. Journal of Physics C: Solid State Physics, 17, L31.
518 Mombourquette, M.J., and Weil, J.A. (2006) EPR-NMR user's manual. University of
519 Saskatchewan, Saskatoon.
520 Nassau, K. (2001) The Physics and Chemistry of Color: The Fifteen Causes of Color, 496 p. Wiley-
521 VHC.
522 Pake, and Estle (1973) The physical principles of electron paramagnetic resonance. W. A Benjamin.
523 Requardt, A., Hill, F., and Lehmann, G. (1982) A Firmly Localized Hole Center in the Mineral
524 Brazilianite NaAl3(PO4)2(OH)4. Zeitschrift für Naturforschung A, 37, 280–286.

525 Schirmer, O.F. (2006) O − bound small polarons in oxide materials. Journal of Physics: Condensed
526 Matter, 18, R667–R704.
527 Schmitz, B., Jakubith, M., and Lehmann, G. (1979) A Simple and Convenient EPR Standard for
528 Determination of g-Factors and Spin Concentrations. Zeitschrift für Naturforschung A, 34,
529 906–908.
530 Silva, D.N. da, Guedes, K.J., Pinheiro, M.V.B., Spaeth, J.M., and Krambrock, K. (2005) The
531 microscopic structure of the oxygen–aluminium hole center in natural and neutron irradiated
532 blue topaz. Physics and Chemistry of Minerals, 32, 436–441.
533 Spaeth, J.-M., Niklas, J.R., and H., B.R. (1992) Structural analysis of point defects in solids, Solid-
534 Stat. Springer-Verlag.
535 Stoll, S., and Schweiger, A. (2006) EasySpin, a comprehensive software package for spectral
536 simulation and analysis in EPR. Journal of Magnetic Resonance, 178, 42–55.
537

538 **LIST OF FIGURES CAPTIONS**

539

540 **FIGURE 1** - EPR spectra of montebrasite sample: (a) prior to irradiation (b) after gamma
541 irradiation (dose of 200 kGy) and (c) after electron irradiation (dose of 80 MGy) measured at 300 K
542 and with microwave frequency of ~9.46 GHz. The magnetic field was parallel to the **a**-axis. Figures
543 (d-f) show the experimental EPR spectra in black lines together with a fit of the spectra (red lines).
544 For the parameters used in the fits, see text and Table 1. Spectra (d) and (e) were measured at 300 K
545 for a gamma-irradiated sample, whereas the spectrum in (f) was measured at 15 K for the electron-
546 irradiated samples, where its EPR line intensity was larger.. An EPR spectrum of the O^- hole center
547 is shown in (d), whereas the two Ti-related electron centers, Ti^{3+}(I) and Ti^{3+}(II), are shown in (e)
548 and (f) respectively.

549 **FIGURE 2 -** Angular dependence of EPR spectra of montebrasite samples after gamma (200 kGy)
550 and electron (80 MGy) irradiation measured in three mutual perpendicular crystal planes: P1:

c*b*c*, P2: **c*ac*** and P3: **b*ab***, at room temperature (a-c), for the O^- and the Ti^{3+}(I) centers. Figures (d-f) show angular dependences of the EPR spectra of the Ti^{3+}(II) center in the electron irradiated sample, measured at 15K and in the same three planes. The colored lines indicate the spectra when the magnetic field is along the crystal directions **a** (orange), $\mathbf{b}^*$ (blue) and $\mathbf{c}^*$ (red). For the low temperature measurements, the O^- lines, despite being partially saturated, are still visible at the lower fields.

FIGURE 3 - Fit of the EPR angular dependences of the montebrasite sample in three mutual perpendicular crystal planes: P1: **c*b*c***, P2: **c*ac*** and P3: **b*ab***. The black dots represent the center of the line positions shown in the Figure 2, and the red solid lines are from the fit of the spin Hamiltonian of eq. 1 using exact diagonalization. The Figures (a-c), are for the O^- centers while the (d-f) for the Ti^{3+}(I) centers, all measured at room temperature. Figures (g-i) represent the fit of the EPR angular dependences for the Ti^{3+}(II) center measured at 15K and in the same three planes.

FIGURE 4 – Concentrations in ppm (wt.) of the O^- (black triangle) and Ti^{3+} (I) (red circle) (a) as a function of the gamma-irradiation dose and (b) as a function of the isochronal annealing temperature (30 min.) measured for AAM sample after gamma irradiation.

FIGURE 5 – Optical absorption spectra in the UV-VIS spectral range of non-irradiated and e^--irradiated montebrasite sample measured at room temperature. The spectra were artificially displaced for better view. The inset shows a photo of the electron-irradiated sample exhibiting the greenish-blue color and the non-irradiated colorless sample.

FIGURE 6 – Atomic structure of the three paramagnetic centers identified in gamma- and electron-irradiated montebrasite: a) the O^- center; b) the Ti^{3+}(I) center; and c) the Ti^{3+}(II) center. The color coding for the ions/molecules are as follow: blue (Al^{3+}), red (O^{2-}), orange (Ti^{3+}) and white (OH^-). The two nearly equivalent Al neighbors are indicated as Al1 and Al2. The *g* and hyperfine tensor

575 ellipsoids, as well as the arrows representing their principal **z**-axes directions are shown in green
576 and blue, respectively.

This is a preprint, the final version is subject to change, of the American Mineralogist (MSA)
Cite as Authors (Year) Title. American Mineralogist, in press.
DOI: https://doi.org/10.2138/am-2020-7168

577 **TABLES**

578

579 **TABLE 1 –** Spin Hamiltonian parameters and their errors of O^- hole centers and the Ti^{3+}(I) and
580 Ti^{3+}(II) electron centers in gamma (Ti^{3+} (I) centers) and electron (Ti^{3+} (II) center) irradiated
581 montebrasite: principal values and directions (given by polar angles Θ (zenite) and Φ (azimute) in
582 relation of ***a***-axis) of *g* tensor. All data used in the analysis were collected at 300 K, with exception
583 of the data used for the Ti^{3+}(II) analysis (collected at 15 K). The *g*-tensors of O^- centers derived
584 from the analysis of the angular dependencies for the electron and gamma-irradiated samples are
585 compared.

This is a preprint, the final version is subject to change, of the American Mineralogist (MSA)
Cite as Authors (Year) Title. American Mineralogist, in press.
DOI: https://doi.org/10.2138/am-2020-7168

O^- hole center									
	Gamma-irradiated sample – 300 K					**Electron-irradiated sample – 300 K**			
	g-tensor			**2 × ^{27}Al shf (MHz)**		**g-tensor**			
	g_{xx}	**g_{yy}**	**g_{zz}**	**a/h**	**b/h**	**g_{xx}**	**g_{yy}**	**g_{zz}**	
	1.9946 (2)	2.0075 (2)	2.0280 (2)	-18.1 (1)	1.1 (1)	1.9930 (2)	2.0049 (2)	2.0270 (1)	
Θ	53 (1)	141 (1)	78 (1)			50 (1)	40(1)	92 (1)	
Φ	106 (1)	131 (1)	205 (1)			355 (1)	179 (1)	267 (1)	
Ti^{3+} (I)									
Gamma-irradiated sample - 300 K									
	g-tensor			**^{47,49}Ti hf(MHz)**					
	g_{xx}	**g_{yy}**	**g_{zz}**	**A_{xx}/h**	**A_{yy}/h**	**A_{zz}/h**	**a/h**	**b/h**	**b'/h**
	1.9294 (1)	1.9386 (1)	1.9532 (1)	20.1 (9)	21.0 (7)	25.2 (7)	22 (2)	1.5 (2)	0.4 (1)
Θ	57 (1)	44 (1)	64 (1)	71 (1)	87 (1)	19 (1)	**A_{hf}/h (MHz) for B // a**		
Φ	253 (1)	121 (1)	1 (1)	253 (1)	162 (1)	62 (1)	46.5 (1)		
							2 × ^{1}H A_{hf}/h (MHz) for B // a		
							24.9 (1)		
Ti^{3+} (II)									
Electron-irradiated sample - 15 K									
	g-tensor						**^{47,49}Ti hf (MHz) for B // a**		
	g_{xx}	**g_{yy}**	**g_{zz}**				83.1 (1)		
	1.782 (3)	1.873 (4)	1.951 (2)						
Θ	32 (1)	58 (1)	91 (1)						
Φ	348 (1)	167 (1)	77 (1)						

586

This is a preprint, the final version is subject to change, of the American Mineralogist (MSA)
Cite as Authors (Year) Title. American Mineralogist, in press.
DOI: https://doi.org/10.2138/am-2020-7168

Figure 1

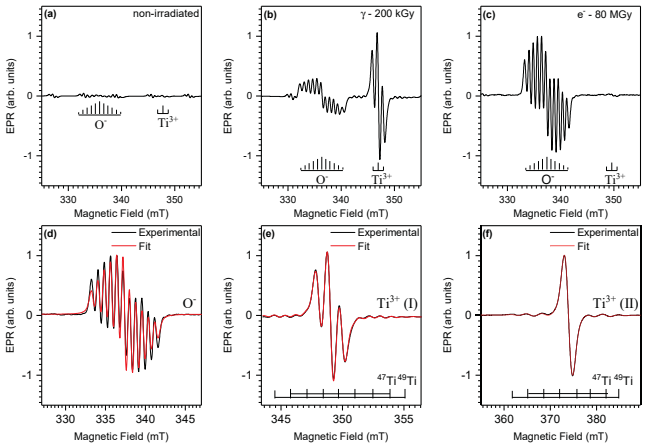

Figure 2

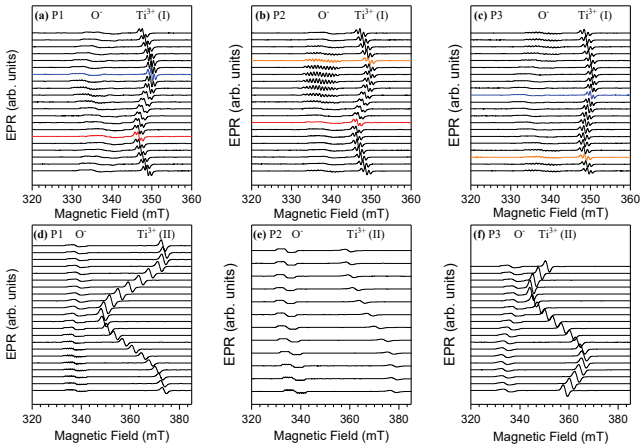

Figure 3

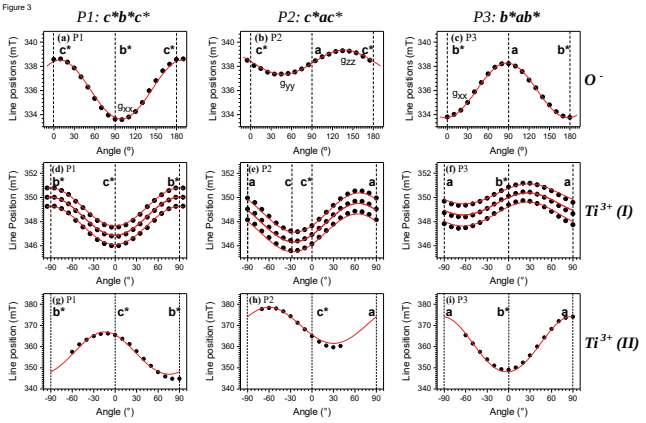

This is a preprint, the final version is subject to change, of the American Mineralogist (MSA)
Cite as Authors (Year) Title. American Mineralogist, in press.
DOI: https://doi.org/10.2138/am-2020-7168

Figure 4

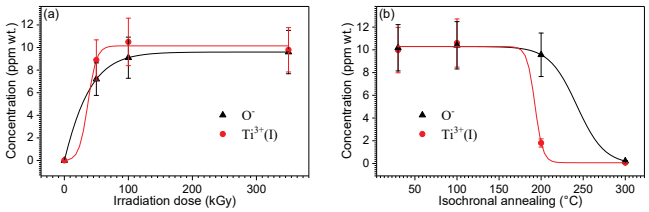

This is a preprint, the final version is subject to change, of the American Mineralogist (MSA)
Cite as Authors (Year) Title. American Mineralogist, in press.
DOI: https://doi.org/10.2138/am-2020-7168

Figure 5

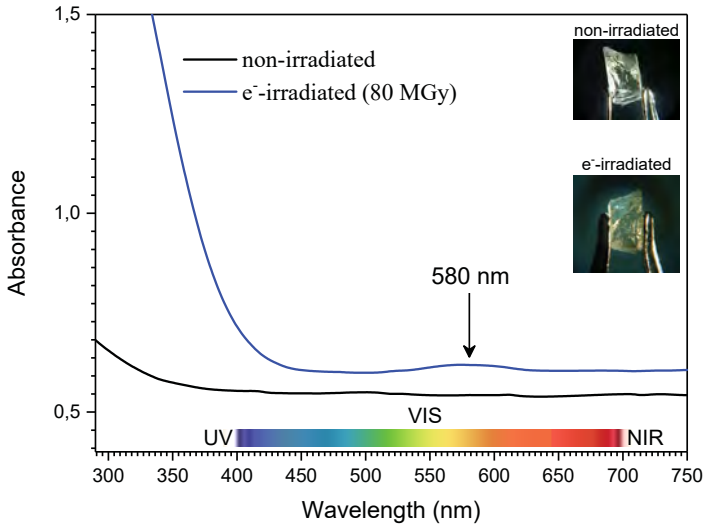

This is a preprint, the final version is subject to change, of the American Mineralogist (MSA)
Cite as Authors (Year) Title. American Mineralogist, in press.
DOI: https://doi.org/10.2138/am-2020-7168

Figure 6